Sound & Vibration 2026, 60(5), 2029.
doi: https://doi.org/10.59400/sv2029

Article

Influence of parameter changes on honeycomb structure debonding detection based on band gap method

Ye Yuan[1], Bin Liu[1,2,*], Chengyou Lei[3], Zhiguo Zhang[4,*]

[1] Institute of Acoustics, Chinese Academy of Sciences, Beijing 100190, China
[2] University of Chinese Academy of Sciences, Beijing 100049, China
[3] Wuhan Second Ship Design and Research Institute, Wuhan 430200, China
[4] School of Instrumentation Science and Engineering, Harbin Institute of Technology, Harbin 150001, China
* **Corresponding author:** Bin Liu, bin.liu@mail.ioa.ac.cn; Zhiguo Zhang, zhangzhiguo@hit.edu.cn

CITATION

Yuan Y, Liu B, Lei C, et al. Influence of parameter changes on honeycomb structure debonding detection based on band gap method. Sound & Vibration. 2026; 60(5): 2029. https://doi.org/10.59400/sv2029

ARTICLE INFO

Received: 11 November 2024
Revised: 3 February 2025
Accepted: 11 February 2025
Available online: 23 July 2026

Abstract: Honeycomb structures have been widely used in many industrial fields due to their excellent properties. However, it is always challenging to rapidly and accurately detect defects such as debonding in the structure, especially in the in-service situation. In response to this, we have proposed an acoustic testing method without coupling agents based on the acoustic band gap feature in the structure. However, the influence of test parameters such as signal excitation and reception on the band gap feature has not been comprehensively and thoroughly investigated, and the parameters have not been optimized. In this paper, the transmission frequency response (TFR) curves were measured, and the band gap features were investigated at different parameters. The results demonstrated that the band gap feature changes a little with the pressure between the probes and the specimen, the amplitude of the exciting signal, the sweep duration, and the detection direction. While it changes significantly with the exciting-receiving distance. Experimental results demonstrated that to form a stable band gap feature, the wave should propagate through at least three honeycomb unit widths before being received. Further analysis indicates that the defect resolution of the proposed method is about two honeycomb unit widths. This work can be used to select the proper detection parameters and further improve the reliability and efficiency of this technique.

Keywords: honeycomb structure; band gap; debonding defect; nondestructive testing; detection parameters

1. Introduction

Honeycomb structures are widely used in transportation, aerospace, and other fields for their excellent material properties [1–4]. However, various different defects are inevitably introduced due to factors of manufacturing process and working environment. Therefore, timely inspection of the structure is required to prevent major safety hazards due to structural failure. In particular, for in-service inspection methods of honeycomb structures, it is first desirable to have both detection efficiency, sensitivity and suitability. However, the characteristics of traditional inspection methods, such as ultrasonic C-scan [5, 6], radiographic inspection [7], infrared thermography [8, 9], Lamb wave [10, 11], and acoustic emission [12, 13], as shown in **Table 1**, can hardly meet these requirements at the same time [14–17].

Table 1. Advantages and disadvantages of in-service inspection for honeycomb structures.

Nondestructive testing methods	Advantages	Disadvantages
Radiographic testing	Sensitive to defects with large density variations (water accumulation, foreign objects, etc.), high efficiency	Difficult to detect debonding defects, requires radiation protection and expensive equipment.
ultrasonic C-scan	Sensitive to debonding defects	Low efficiency, need coupling agent. Even using laser-ultrasound or air-coupled ultrasound does not solve the problem of low acoustic conversion efficiency.
Acoustic emission	High efficiency, suitable for online monitoring.	Vulnerable to background noise, only sensitive to cracks that are propagating.
Thermography	High efficiency	Strongly influenced by environmental factors (such as ambient temperature and wind speed)

The reason for this is that the conventional methods are used to detect defects by comparing local differences in physical properties of the structure, such as local ray absorption [18], thermo-physical properties [19], small displacement deformations [20], and differences in ultrasonic transmission or reflection. When the structure to be tested is large, and at the same time the inspection results require high accuracy, the inspection cost will rise sharply [21]. Therefore, in order to solve the above problems, it is necessary to propose corresponding inspection principles and methods from the properties possessed by the structure itself.

To address this problem, we have proposed a method for detecting debonding defects in honeycomb structures based on the acoustic band gap feature [15]. The band gap method (BGM) takes advantage of the spatial periodicity of honeycomb structure, which can prevent elastic waves in part of the frequency range from propagating through the structure, a phenomenon known as acoustic band gap. On the other hand, if the spatial periodicity is disrupted, such as in the case of debonding defect, the band gap will disappear. The results have indicated that, while ensuring detection efficiency, BGM does not require complex algorithms or expensive equipment, nor does it need coupling agents, demonstrating its potential for in-service testing.

To further investigate the effectiveness of the BGM, it is essential to examine the factors influencing the detection of the band gap feature and to discuss the method's defect discrimination ability. According to studies related to phononic crystals [22–24], the band gap is one of the important properties resulting from the modulation effect of the periodic structure on the acoustic wave [25–27]. Additionally, many works have demonstrated that the attenuation degree of elastic wave in the band gap frequency range is intensively determined by the distance the wave has propagated through the material [28–30]. However, it should be emphasized that all the above studies are only to confirm the existence of band gap in periodic structures, yet a systematic study about the influence of excitation and reception parameters on band gap detection is not available. Therefore, the influence of detection parameters on wave propagation in honeycomb structure and how to select the appropriate parameters to obtain more reliable results and improve the detection efficiency need further research and analysis.

In this paper, the influence of the detection parameters on the elastic wave propagation characteristics in the honeycomb structure, especially on the band gap feature, has been investigated. The transmission frequency response (TFR) curves with different excitation and reception parameters, such as the pressure between the probes and the specimen, the amplitude of the exciting signal, the sweep duration, the detection direction, and the exciting-receiving distance, were measured in both intact and debonding areas. The reason for the observed phenomena was analyzed, and the parameter selection range or standard was suggested based on the analysis.

2. Method and materials

2.1. Materials and specimen fabrication

The honeycomb structure consists of upper and bottom skins and a honeycomb core, which are made of nickel-based high-temperature alloy (Haynes 214). The material properties are characterized by Young's modulus $E = 218$ GPa, Poisson's ratio $\mu = 0.3$, and density $\rho = 8{,}050$ kg/m^3. A rectangular honeycomb plate (220 mm × 150 mm) was fabricated as shown in **Figure 1a**. The thickness of the skin and the height of the core are 0.2 mm and 4.1 mm, respectively. The wall of the core is 0.1 mm in thickness and 4 mm in side length. The nickel-based brazing alloy was used to braze the skins and the honeycomb core. Meanwhile, the artificial debonding defects were introduced by removing the adhesive film between the skin and core at the corresponding debonding location. To investigate the proposed method for damage evaluation with size changing, the diameter of the debonding defect is 35 mm, 25 mm, 20 mm, 10 mm, 8 mm, and 5 mm in order from the largest to the smallest.

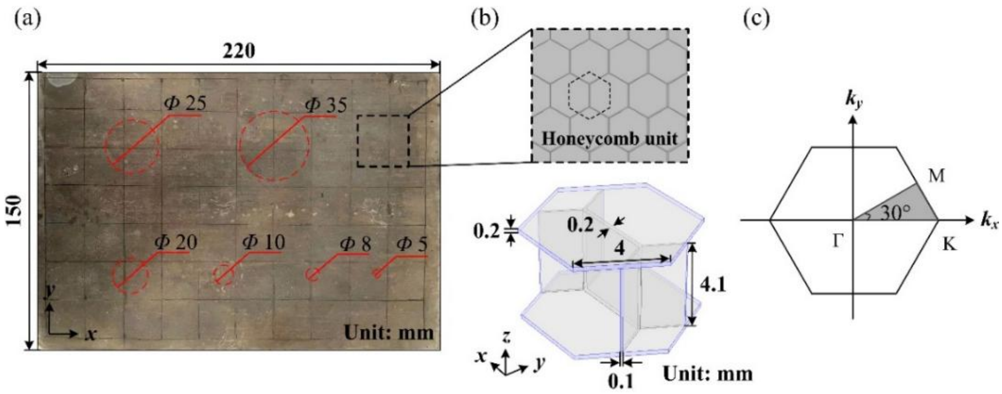

Figure 1. **(a)** The specimen; **(b)** Honeycomb unit; **(c)** The first irreducible Brillouin zone.

2.2. Experimental setup and method

Based on the above geometric and material parameters of the honeycomb structure, the model was constructed using three-dimensional solid elements in COMSOL Multiphysics to obtain the dispersion relation. A Floquet periodic boundary condition (as shown in the blue area of the unit cell in **Figure 1b**) was applied to the interfaces between the nearest unit cells to realize periodic extension. According to the Bloch–Floquet theorem:

$$u\left(r+R_{\mathrm{n}}\right)=u(r)e^{ik\cdot R_{\mathrm{n}}}. \tag{1}$$

Where u represents the elastic wave function, k is the Bloch wave vector, and R_{n} is the lattice vector. The Bloch wave vector was set in the first irreducible Brillouin zone (as shown in the gray area in **Figure 1c**).

To reveal the transmission frequency response in a honeycomb structure, an experimental investigation was carried out with the schematic diagram illustrated in **Figure 2**. In this experimental setup, a piezoelectric actuator (Thorlabs, PA4HKW), which was driven by a signal generator (RIGOL, DG811), generated the acoustic waves used for excitation. An accelerometer (PCB Piezotronics, 352C33) was employed to receive the wave passing through the honeycomb structure. It should be noted that the accelerometer needs a constant current source (Art, SIT_IPEP) to drive. In the detection processing, the dry coupling between the probes and the specimen was used for detection due to the working principle of the probes. To ensure that the probes are in full contact with the specimen and to prevent excessive pressure from damaging the probes and the specimen, a pressure sensor (Daysensor, DYHW-108) was utilized to measure and control the pressure between them. A fixture was made to hold all the sensors on it and also facilitate its mounting on a robotic arm (AUBO, i5). This robotic arm realized automatic detection of the specimen as an action actuator. Then the measurement signal and pressure signal were transferred to the computer for processing through a data acquisition card (Fcctec, FCFR-usb2160). Finally, the corresponding programs were written in LabVIEW and Python to implement functions such as data acquisition, storage, processing, and control of the robotic arm.

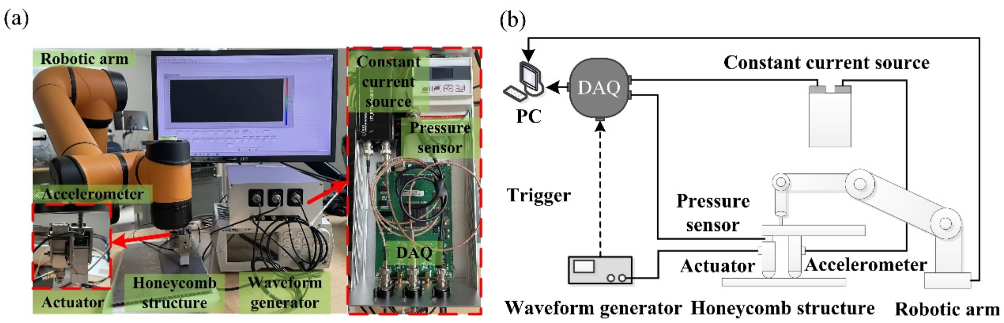

Figure 2. **(a)** Photograph of experimental devices; **(b)** Schematic of experimental setup.

To assess the transmission properties of the honeycomb structure, the TFR is determined as follows:

$$TFR_m = 20\log\left[\frac{S_1(\omega)}{H_s(\omega)}\right]. \tag{2}$$

where $H_s(\omega)$ represents the system function, which is determined through measurements conducted using the piezoelectric actuator and accelerometer in direct contact with each other. Meanwhile, $S_1(\omega)$ denotes the signal received within the honeycomb structure through this system.

3. Results and discussion

3.1. Calculation simulation and experimental verification of band gap

The dispersion relation of the honeycomb structure was given in our previous study. The modes of band branches and the coupling relations between them have been analyzed in detail. In this work, only the three band branches where modes A_0, R_{PS}, and R_{PA} are located that have a direct effect on band gap formation were presented in **Figure 3a**. It can be observed that the band branches where modes R_{PA} and A_0 are located are strongly coupled to each other. The dispersion curve was split into several branches, and a band gap appears from 41 kHz to 48 kHz between the band branches where modes R_{PS} and R_{PA} are located. According to previous studies, it has already been evidenced that the band gap is caused by the localized resonance of the skins, which is restricted by the bond joint [15].

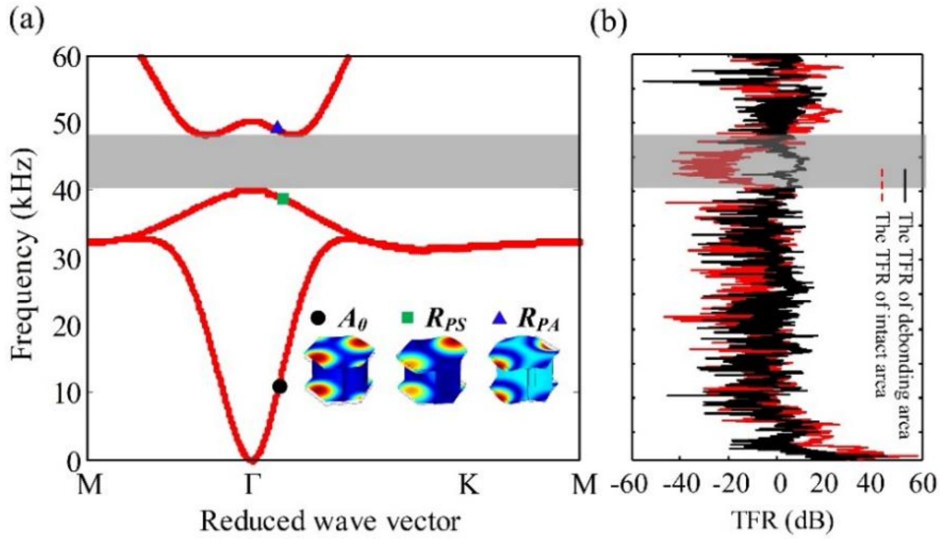

Figure 3. The dispersion curves and transmission frequency response (TFR) of the honeycomb structure: **(a)** Three types of the honeycomb structure below 60 kHz, which are modes R_{PS}, R_{PA} and A_0, respectively. There is a band gap between these branches in the frequency range from about 41 kHz to 48 kHz; **(b)** Measured TFR of intact and debonding areas of honeycomb structure.

To demonstrate the existence of the band gap feature in the honeycomb structure, the TFR curves of intact and debonding areas were measured using the experimental platform in Subsection 2.2. In the detection process, the pressure between the probes and the specimen was usually about 3 N (g = 10 N/kg) to enable the probes to be in full contact with the specimen. A linear sweep signal was used to excite the actuator, and the amplitude of the exciting signal was selected at 5 $V_{p\text{-}p}$. As the band gap is in the frequency range from 41 kHz to 48 kHz, the frequency band of the excitation signal was set from 1 kHz to 60 kHz, and the sweep duration was set to 0.1 s. The distance between the exciting and receiving points was set at 20 mm during measurements. The direction of the exciting-receiving link relative to the specimen is the same as the ΓK line of the first irreducible Brillouin zone (as shown in **Figure 1c**). To facilitate comparison of differences between TFR curves, all of the measured results were normalized by subtracting the average of the TFR curves corresponding to the region without the band gap (20 kHz to 40 kHz).

The measured results are shown in **Figure 3b**, where the red dash-dot line and black solid line denote the TFR curves of intact and debonding areas, respectively. It can be observed that the minimum value of the TFR curve in the intact area reached −30 dB between 41 kHz and 48 kHz. The result demonstrated that there is a band gap in this frequency range. This is consistent with the results of the dispersion curve analysis in **Figure 3a**. Compared to the TFR curve of the intact area, the TFR curve of the debonding area is nearly stable in the measured frequency band. It means that the band gap feature disappeared in the debonding area. Accordingly, the bandgap feature can be applied to detect debonding in the honeycomb structure, which was preliminarily verified.

3.2. The influence of excitation signal type on the band gap feature

The TFR of the honeycomb structure can also be obtained using white noise excitation; the measured results in the intact area and debonding area are shown in **Figure 4**. Compared with the TFR curves of the sweep signal excitation, the band gap feature can hardly be distinguished in the TFR curves of the white noise excitation (as shown in **Figure 4a**). Meanwhile, it is also not easy to distinguish the intact and debonding TFR curves. Therefore, in this paper, in order to clearly observe the band gap feature, the sweep signal is selected as the excitation signal.

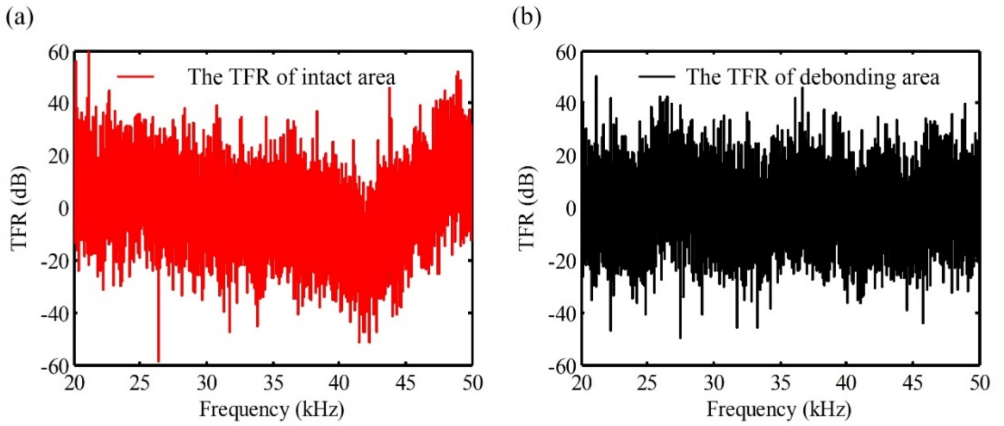

Figure 4. Measurement results of TFR curves excited by white noise: **(a)** Intact area; **(b)** Debonding area.

3.3. The influence of pressure between the probes and the specimen on the band gap feature

In this section, the influence of pressure between the probes and the specimen on the detection result is first investigated. The frequency range of the exciting signal was set from 20 kHz to 50 kHz, which was sufficient to cover the band gap. In this paper, a pressure of 2 N between the probes and the specimen is sufficient to ensure contact between the probes and the specimen. Meanwhile, the pressure should be smaller than 12 N, or the specimen may be damaged by the pressure. Therefore, the pressure between probes and specimen was selected at 3 N, 5 N, 7 N, 9 N, and 10 N, and the other parameters and operation were kept unchanged as in **Figure 3b**. A moving average filter was employed to reduce the effect of noise, and the window length was set to 128. The TFR curves of the intact and debonding areas at different pressures are shown in **Figure 5**. It can be observed that the pressure almost does not affect the results, both in the intact area and the debonding area, within the measured pressure range. Therefore, the pressure is set to 3 N in the following experiments.

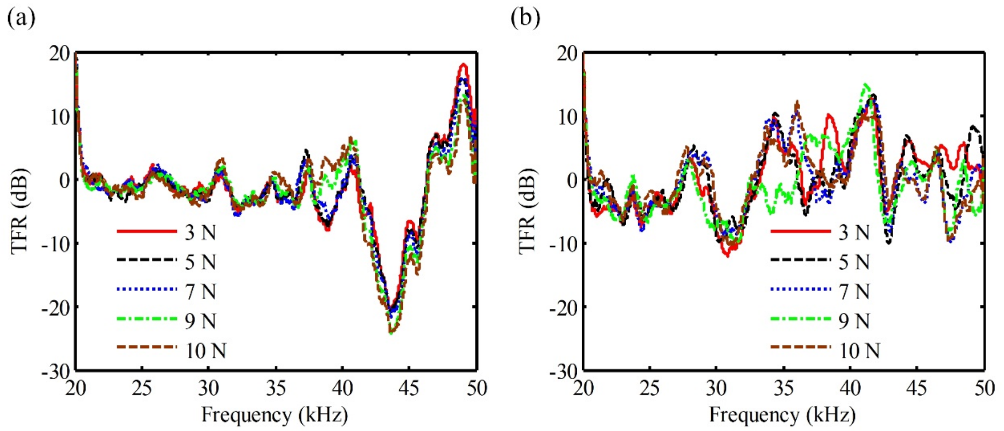

Figure 5. The influence of different pressures between probes and specimen on the detection results: **(a)** The TFR of the intact area; **(b)** The TFR of the debonding area.

3.4. The influence of excitation parameters on the band gap feature

To observe the influence of exciting signal amplitude on the detection results, the amplitudes, 2 $V_{p\text{-}p}$, 4 $V_{p\text{-}p}$, 6 $V_{p\text{-}p}$, 8 $V_{p\text{-}p}$ and 9.9 $V_{p\text{-}p}$, were selected. Other parameters were kept the same as in **Figure 5**. The TFR curves of the intact and debonding areas at different amplitudes are shown in **Figure 6**. It can be observed that the TFR curves are almost unchanged, including the location and values of the peaks and valleys. This result indicates that the amplitude does not affect the measurement results. Therefore, the amplitude can be set to 5 $V_{p\text{-}p}$ in the later experiments.

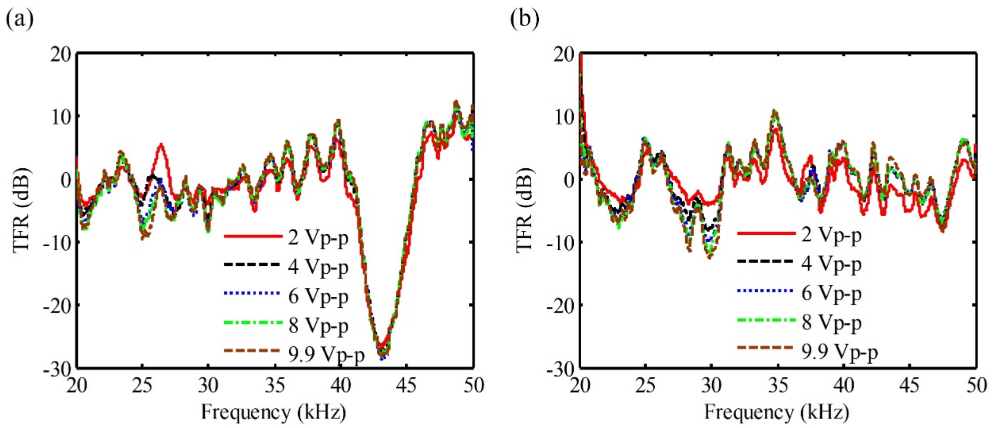

Figure 6. The influence of different amplitudes on the detection results: **(a)** The TFR of the intact area; **(b)** The TFR of the debonding area.

In this part, the influence of sweep duration on the band gap feature is investigated. The sweep durations of 1 s, 0.1 s, 0.01 s, and 0.001 s were selected. Other parameters were kept the same as in **Figure 5**. The TFR curves of the intact and debonding areas at different sweep durations are shown in **Figure 7**. It can be observed that even if the sweep duration is short, which reached 0.001 s, the band gap can still be observed in the TFR of the intact area from 41 kHz to 48 kHz. For the TFR curves of debonding area, there is no significant attenuation in the measured frequency range, and it is relatively steady. To improve detection efficiency, the sweep duration should be shorter. However, it can be observed that when the sweep duration is shorter than 0.001 s, the

TFR feature in the non-band gap range is relatively different. It indicated that a more accurate result can be obtained with a larger sweep duration as the system reaches steady state. Therefore, in the next experiments, the sweep duration was selected at 0.1 s.

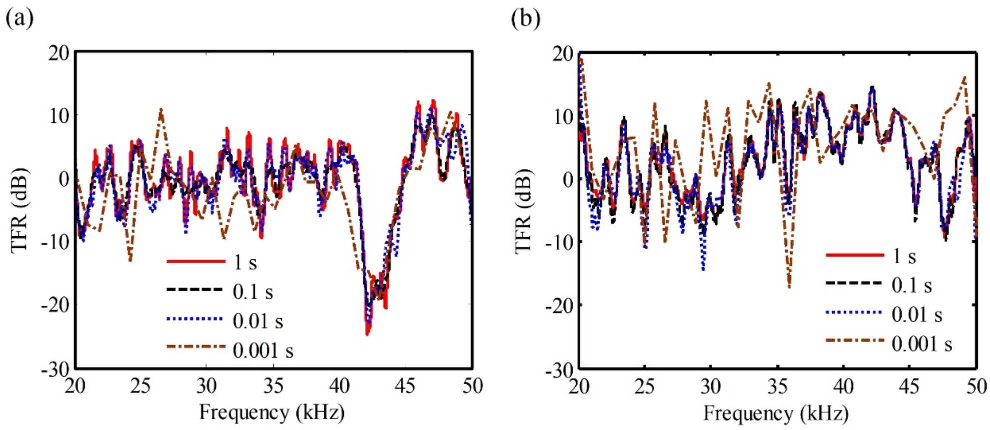

Figure 7. The influence of different sweep durations on the detection results: **(a)** The TFR of the intact area; **(b)** The TFR of the debonding area.

3.5. The influence of receiving parameters on the band gap feature

According to our previous study, the influence of detection direction and exciting-receiving distance on the TFR curves of the intact area has been initially investigated [15]. However, the TFR curves of the debonding area at different angles and exciting-receiving distances have not been measured, and the reasons for the influence of receiving parameters on the band gap were not analyzed. Here, these were measured and analyzed in this work, as shown in **Figures 8** and **9**, respectively.

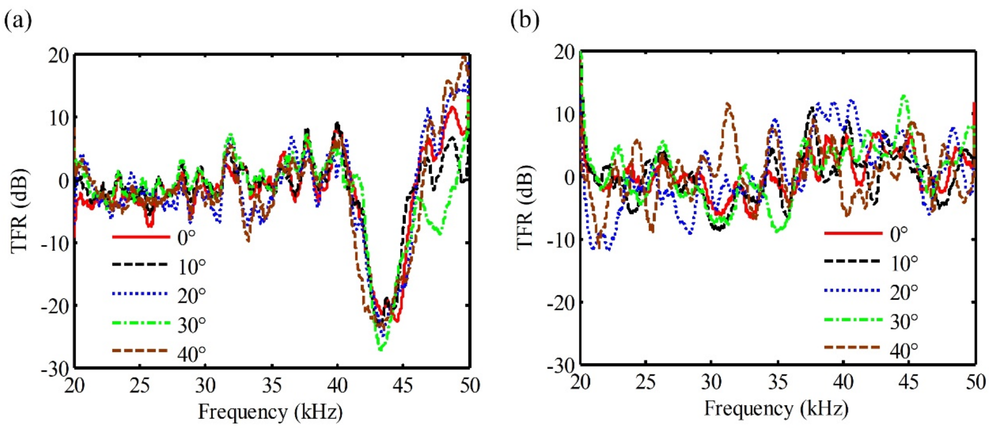

Figure 8. The influence of different wave propagation directions on the detection results: **(a)** The TFR of the intact area; **(b)** The TFR of the debonding area.

Since the angle of the irreducible Brillouin zone is 30° (as shown in **Figure 1c**), to completely cover the irreducible Brillouin zone, the receiving angle was varied clockwise from 0° to 40° in a step size of 10°, with the x-direction as the reference direction. Other parameters were kept the same as in **Figure 5**. The results of the intact and debonding areas at different angles are shown in **Figure 8a,b**, respectively. For the TFR curves of the intact area, it can be observed that there is a larger attenuation of about 25 dB in the range from 41 kHz to 48 kHz than that of other frequency bands for all testing directions. In the debonding area, there was no band gap feature, and the TFR curve varied slightly in all directions.

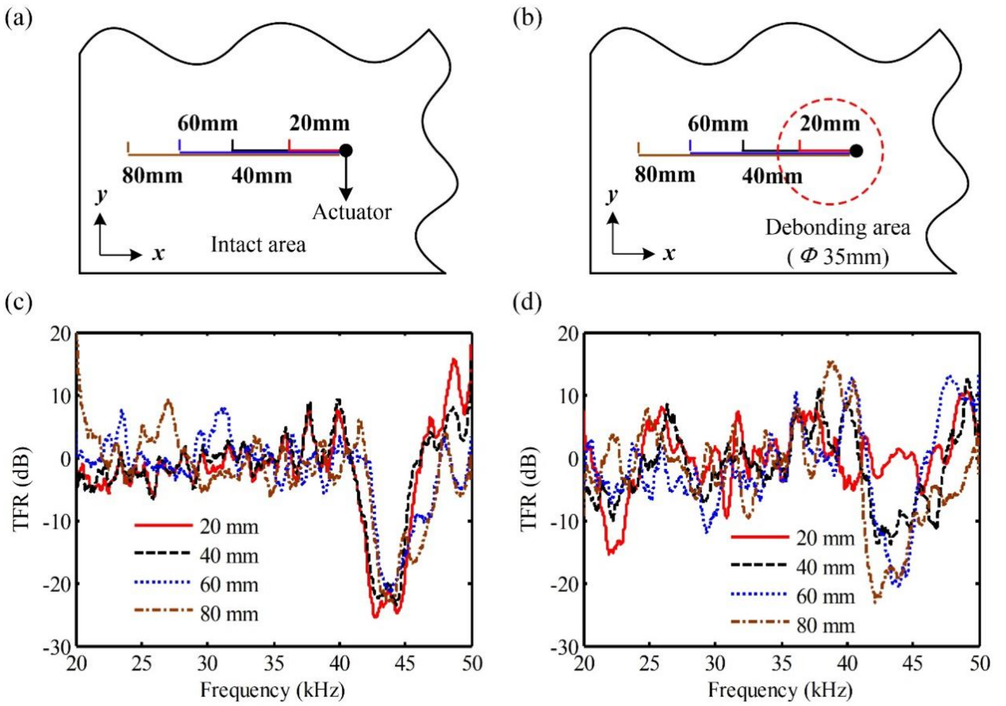

Figure 9. The influence of exciting-receiving distance on the detection results: **(a)** Diagram of different exciting-receiving distances in the intact area; **(b)** Diagram of different exciting-receiving distances in the debonding area; **(c)** The TFR curves of the intact area; **(d)** The TFR curves of the debonding area.

According to the dispersion relation (as shown in **Figure 3a**), it is suggested that the band gap is a complete band gap, that is, the larger attenuation in the range from 41 kHz to 48 kHz will exist without exception when the wave propagates in different directions in the structure. Therefore, the experimental results verify the validity of the theoretical analysis and also indicate that the angle has little effect on the TFR curves.

As mentioned before, previous works indicated that the band gap features are intensively affected by the wave propagation distance in the material [28–30]. Next, the influence of exciting-receiving distance is further investigated in this part. **Figure 9a**,**b** show the schematic diagrams of different exciting-receiving distances in the intact area and debonding area, respectively. In **Figure 9a**, the position of the actuator (exciting probe) was fixed, and the measurements were performed at exciting-receiving distances of 20 mm, 40 mm, 60 mm, and 80 mm, respectively. In **Figure 9b** the actuator was fixed in the 35 mm-diameter defect, the fixed position was 8 mm from the boundary. The results of intact and debonding areas were shown in **Figure 9c**,**d**. The red, black, blue, and brown lines represented the TFR curves at distances of 20 mm, 40 mm, 60 mm, and 80 mm, respectively.

In **Figure 9c**, it can be noted that even at an exciting-receiving distance of 20 mm, the TFR in the band gap range reaches an attenuation of about 24 dB compared to the other frequency bands. These results indicate that the wave attenuates strongly in the range from 41 kHz to 48 kHz, and the elastic wave energy in this frequency range can hardly propagate over a distance of 20 mm (about three honeycomb unit widths). It can also be noted that the attenuation in the band gap slightly increases at distances greater than 20 mm, and the attenuation almost keeps unchanged when it reaches about 25 dB.

In **Figure 9d**, the results show that the minimum value of TFR between 41 kHz and 48 kHz changes from −5 dB to −23 dB as the distance increases. It can be observed that the TFR curve is relatively steady when the distance is 20 mm. There is no significant attenuation in the range of 41 kHz to 48 kHz compared to the other frequency bands, i.e., no band gap is observed in this detection area (both excitation and reception probes are on the debonding defect). But at a distance of 40 mm (with the receiving probe in the intact area), the TFR curves in the range of 41 kHz and 48 kHz exhibit a tendency to attenuation, about −13 dB. Moreover, the attenuation increases slightly with the distance of the acoustic wave propagating in the intact area as the distance increases (approximately −19 dB to −22 dB when the distance changes from 60 mm to 80 mm).

According to **Figure 9c**,**d**, it is suggested that the band gap feature can be identified at a distance of 20 mm, and that the feature does not change significantly with increasing distance. For the detection of debonding defects, it is suggested that the exciting-receiving distance D should be smaller than the debonding size, or it might be difficult to distinguish the defect signal from the intact signal.

From the above analysis, the smaller the detection distance, the higher the resolution of the defect. Since the actuator and accelerometer have a certain size, it is difficult to further reduce the distance between the two probes to less than 20 mm. However, according to the previous results, especially in **Figure 9d**, we note that the debonding area basically does not cause attenuation in the frequency range from 20 kHz to 50 kHz. Further, when part of the acoustic wave propagation path is in the debonding area and the other part is in the intact area, the TFR curve measured in this case can be considered as the TFR curve in the intact part. Thus, the measurement of TFR curves for different exciting-receiving distances in the intact area can be realized in this way. In order to obtain the optimal detection distance in the honeycomb structure and the detection resolution for defects, a more in-depth study was conducted with the experimental settings shown in **Figure 10a**: The exciting-receiving distance D was fixed at 30 mm on a 35 mm-diameter defect. The detection positions are divided into the following two types: Type 1: exciting point in the debonding area; receiving point is in the intact area and d = 7 mm, 14 mm, and 21 mm from the edge of the debonding defect, which is about 1, 2, and 3 widths of honeycomb units. Type 2: Both exciting and receiving points are in the intact area; at this time, d = 30 mm.

To improve the reliability of the test results, all positions are measured three times and averaged to obtain the TFR curves. The results are shown in **Figure 10b**. It can be observed that as the number of acoustic waves propagating through the honeycomb units increases, the attenuation of TFR in the bandgap range changes from 13 dB to 25 dB compared to the other frequency bands. This suggests that the formation of band gap features is related to the number of acoustic waves propagating through the honeycomb units. In fact, the band gap feature can be faintly observed even when the acoustic wave propagates through one or two honeycomb units. The band gap range and attenuation reach stability when the acoustic wave propagates through three or more honeycomb units.

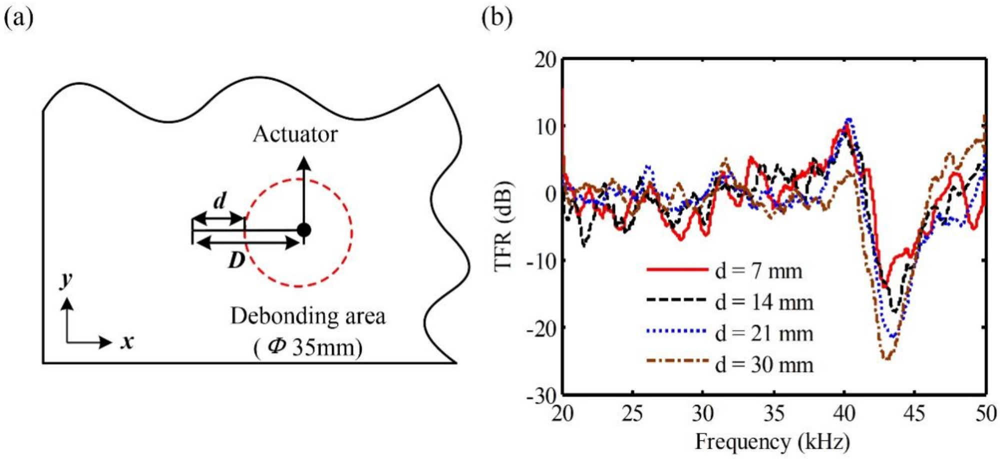

Figure 10. The influence of acoustic wave propagation in different numbers of honeycomb units on the detection results: **(a)** Experimental schematic of acoustic wave propagation in different numbers of honeycomb units; **(b)** Measured TFR curves with different numbers of honeycomb units (d = 7, 14, 21, 30 mm).

This is similar to the results of other researchers studying the band gap [28–30]. Shen and Cao [28] investigated a finite one-dimensional layered medium containing two different periods. The results demonstrated that the acoustic band gap can be formed using only 3 to 4 period units. Al Ba'ba'a et al. [29] used transfer functions to comprehend the formation of band gaps in locally resonant acoustic metamaterials. The results demonstrated that the attenuation of the band gap increases with the number of periodic units the acoustic wave propagated through. Zouari et al. [30] investigated the flexural wave propagation characteristics of a 2D periodic structure. The results shown that the attenuation of the Bragg band gap is about −12 dB when the acoustic wave propagates for 1 to 3 units; the attenuation varies from −15 dB to −35 dB when the acoustic wave propagates for 4 to 6 units.

According to the measured results of this work, the local resonance bandgap of flexural waves in honeycomb structures has a similar phenomenon: the acoustic wave propagates through one unit with a relatively obvious attenuation, while the band gap features are basically stable when the acoustic wave propagates through three or more units. Therefore, combined with the experimental results in this work, it is demonstrated that at least three honeycomb units are required to detect a stable band gap feature. The exciting-receiving distance should be determined as follows:

$$D \geq 3d_h, \tag{3}$$

where D is the exciting-receiving distance and d_h is the width of the honeycomb unit.

To verify the validity of the above conclusions, an aluminum honeycomb structure with a honeycomb core side length of 6 mm was fabricated and tested (the detailed test procedure and results were described in **Appendix A**). The aluminum honeycomb structure has a band gap between 30 kHz and 40 kHz. The results also indicated that it requires the acoustic wave to propagate through at least three honeycomb units to form a stable band gap feature.

The detection resolution of the BGM can also be obtained from the above results. In **Figure 10b**, it should be noted that the difference between the exciting-receiving distance and the defect's diameter cannot exceed the two honeycomb unit widths, preferably not more than one. Therefore, the defect resolution of the BGM for detecting debonding defects in honeycomb structures can be determined as follows:

$$D - d_{re} \leq d_h. \tag{4}$$

In this work,

$$d_{re} \geq 2d_h, \tag{5}$$

where d_{re} is the size of the smallest defect that can be detected.

This conclusion also provides an explanation for our previous work [15], where the scan results could only identify defects with a diameter of 20 mm or more. Since the exciting-receiving distance during the detection process is 20 mm, for a defect with a diameter of 20 mm, the excitation probe and the receiving probe can be completely located in the debonding area, and then the band gap feature disappears in the TFR curve, while for a defect with a diameter of 10 mm, the excitation probe and the receiving probe can only be at most one in the debonding area, at which time the acoustic wave can propagate at least 10 mm in the intact area, which is about 1.5 honeycomb unit widths. According to the results in **Figure 10**, it can be observed that the TFR curve in the band gap range has an obvious attenuation. At this time, it is difficult to distinguish the difference between the TFR curves in the intact and debonding areas. Therefore, defects with a diameter of 10 mm cannot be effectively detected.

4. Conclusion

In summary, this paper focuses on the influence of excitation and reception parameters on the band gap feature and analyzes the reasons for the effects of these parameters. The experimental results demonstrated that pressure between the probes and the specimen, amplitude of the exciting signal, and sweep duration do not affect the measurement results within a reasonable parameter range. Due to the complete band gap, the detection direction also hardly affects the detection results in the honeycomb structure. The exciting-receiving distance is the key parameter for effective defect detection. It is experimentally demonstrated that the band gap feature requires acoustic wave propagation through a minimum of three honeycomb unit widths to be stably represented. Further analysis shows that the defect resolution of the BGM is about two honeycomb unit widths. This study provides the basis for selecting the appropriate detection parameters in a debonding defect detection method based on the BGM. It also helps to improve the detection reliability of this technique. Besides the honeycomb structures, this technology can also be applicable to other structures with spatial periodicity, such as grid structures, corrugated tubes and railway tracks. It is important to note that although structures with different parameters (material, geometry) and configurations may not have a bending wave bandgap, which may limit the application of the method. However, more wave propagation characteristics, such as negative group velocity [31] and zero group velocity [4] could be discovered and used for defect detection by taking advantage of structures' space periodicity.

Author contributions: Conceptualization, YY and BL; methodology, YY and BL; software, YY and BL; validation, YY; formal analysis, BL; investigation, YY and BL; resources, BL and ZZ; data curation, YY; writing—original draft preparation, YY; writing—review and editing, BL, ZZ and CL; visualization, YY; supervision, BL and ZZ; project administration, BL and ZZ; funding acquisition, BL and ZZ. All authors have read and agreed to the published version of the manuscript.

Funding: This research was funded by the National Natural Science Foundation of China, grant number 51805528.

Institutional review board statement: Not applicable.

Informed consent statement: Not applicable.

Data availability statement: Data will be made available on request.

Conflict of interest: The authors declare no conflict of interest.

AI use statement: The authors declare that no artificial intelligence (AI) tools were used in the preparation of this manuscript.

References

1. Wang Z. Recent advances in novel metallic honeycomb structure. Composites Part B: Engineering. 2019; 166: 731–741. doi: 10.1016/j.compositesb.2019.02.011
2. Qi C, Jiang F, Yang S. Advanced honeycomb designs for improving mechanical properties: A review. Composites Part B: Engineering. 2021; 227: 109393. doi: 10.1016/j.compositesb.2021.109393
3. Zhang Q, Yang X, Li P, et al. Bioinspired engineering of honeycomb structure—Using nature to inspire human innovation. Progress in Materials Science. 2015; 74: 332–400. doi: 10.1016/j.pmatsci.2015.05.001
4. Yuan Y, Liu B, Sha Z, et al. Zero group velocity feature in CFRP-Nomex honeycomb structure and its use for debonding detection. Mechanical Systems and Signal Processing. 2024; 216: 111479. doi: 10.1016/j.ymssp.2024.111479
5. Růžek R, Lohonka R, Jironč J. Ultrasonic C-Scan and shearography NDI techniques evaluation of impact defects identification. NDT & E International. 2006; 39(2): 132–142. doi: 10.1016/j.ndteint.2005.07.012
6. Zhang H, Liu S, Rui X, et al. A skin-core debonding quantitative algorithm based on hexagonal units reconstruction for air-coupled ultrasonic C-scan images of honeycomb sandwich structure. Applied Acoustics. 2022; 198: 108964. doi: 10.1016/j.apacoust.2022.108964
7. Kolkoori S, Wrobel N, Zscherpel U, et al. A new X-ray backscatter imaging technique for non-destructive testing of aerospace materials. NDT & E International. 2015; 70: 41–52. doi: 10.1016/j.ndteint.2014.09.008
8. Rellinger T, Underhill PR, Krause TW, et al. Combining eddy current, thermography and laser scanning to characterize low-velocity impact damage in aerospace composite sandwich panels. NDT & E International. 2021; 120: 102421. doi: 10.1016/j.ndteint.2021.102421
9. Zhao H, Zhou Z, Fan J, et al. Application of lock-in thermography for the inspection of disbonds in titanium alloy honeycomb sandwich structure. Infrared Physics & Technology. 2017; 81: 69–78. doi: 10.1016/j.infrared.2016.12.020
10. Sikdar S. Multi-level nondestructive analysis of joint-debond effects in sandwich composite structure. Polymer Testing. 2019; 80: 106149. doi: 10.1016/j.polymertesting.2019.106149
11. Gao F, Wang L, Hua J, et al. Application of Lamb wave and its coda waves to disbond detection in an aeronautical honeycomb composite sandwich. Mechanical Systems and Signal Processing. 2021; 146: 107063. doi:

10.1016/j.ymssp.2020.107063
12. Abdulaziz AH, Hedaya M, Elsabbagh A, et al. Acoustic emission wave propagation in honeycomb sandwich panel structures. Composite Structures. 2021; 277: 114580. doi: 10.1016/j.compstruct.2021.114580
13. Sikdar S, Mirgal P, Banerjee S, et al. Damage-induced acoustic emission source monitoring in a honeycomb sandwich composite structure. Composites Part B: Engineering. 2019; 158: 179–188. doi: 10.1016/j.compositesb.2018.09.071
14. Ma B, Zhou Z, Zhao H, et al. Characterisation of inclusions and disbonds in honeycomb composites using non-contact non-destructive testing techniques. Insight—Non-Destructive Testing and Condition Monitoring. 2015; 57(9): 499–507. doi: 10.1784/insi.2015.57.9.499
15. Yuan Y, Liu B, Jia H, et al. A novel nondestructive testing method for honeycomb structure using acoustic band gap. Mechanical Systems and Signal Processing. 2023; 188: 110053. doi: 10.1016/j.ymssp.2022.110053
16. Wang B, Zhong S, Lee TL, et al. Non-destructive testing and evaluation of composite materials/structures: A state-of-the-art review. Advances in Mechanical Engineering. 2020; 12(4). doi: 10.1177/1687814020913761
17. Asif M, Khan MA, Khan SZ, et al. Identification of an effective nondestructive technique for bond defect determination in laminate composites—A technical review. Journal of Composite Materials. 2018; 52(26): 3589–3599. doi: 10.1177/0021998318766595
18. Hungler PC, Bennett LGI, Lewis WJ, et al. Neutron imaging inspections of composite honeycomb adhesive bonds. Nuclear Instruments and Methods in Physics Research Section A: Accelerators, Spectrometers, Detectors and Associated Equipment. 2011; 651(1): 250–252. doi: 10.1016/j.nima.2011.01.104
19. Liu G, Gao W, Liu W, et al. Debonds and Water-Filled Defects Detection in Honeycomb Sandwich Composites Based on Pulse Infrared Thermography NDT Technique. Russian Journal of Nondestructive Testing. 2023; 59(5): 583–591. doi: 10.1134/S1061830923600089
20. Thomas BP, Annamala Pillai S, Narayanamurthy CS. Investigation on vibration excitation of debonded sandwich structures using time-average digital holography. Applied Optics. 2017; 56(13): F7. doi: 10.1364/AO.56.0000F7
21. Towsyfyan H, Biguri A, Boardman R, et al. Successes and challenges in non-destructive testing of aircraft composite structures. Chinese Journal of Aeronautics. 2020; 33(3): 771–791. doi: 10.1016/j.cja.2019.09.017
22. Lu MH, Feng L, Chen YF. Phononic crystals and acoustic metamaterials. Materials Today. 2009; 12(12): 34–42. doi: 10.1016/S1369-7021(09)70315-3
23. Hussein MI, Leamy MJ, Ruzzene M. Dynamics of Phononic Materials and Structures: Historical Origins, Recent Progress, and Future Outlook. Applied Mechanics Reviews. 2014; 66(4): 040802. doi: 10.1115/1.4026911
24. Maldovan M. Sound and heat revolutions in phononics. Nature. 2013; 503(7475): 209–217. doi: 10.1038/nature12608
25. Meidani M, Kim E, Li F, et al. Tunable evolutions of wave modes and bandgaps in quasi-1D cylindrical phononic crystals. Journal of Sound and Vibration. 2015; 334: 270–281. doi: 10.1016/j.jsv.2014.09.010
26. Zen N, Puurtinen TA, Isotalo TJ, et al. Engineering thermal conductance using a two-dimensional phononic crystal. Nature Communications. 2014; 5(1): 3435. doi: 10.1038/ncomms4435
27. Yang S, Page JH, Liu Z, et al. Ultrasound Tunneling through 3D Phononic Crystals. Physical Review Letters. 2002; 88(10): 104301. doi: 10.1103/PhysRevLett.88.104301
28. Shen M, Cao W. Acoustic band-gap engineering using finite-size layered structures of multiple periodicity. Applied Physics Letters. 1999; 75(23): 3713–3715. doi: 10.1063/1.125438
29. Al Ba'ba'a H, Nouh M, Singh T. Formation of local resonance band gaps in finite acoustic metamaterials: A closed-form transfer function model. Journal of Sound and Vibration. 2017; 410: 429–446. doi: 10.1016/j.jsv.2017.08.009
30. Zouari S, Genevaux JM, Brocail J, et al. Band gap formation in thin plates with a periodic array of resonators. Mechanics & Industry. 2017; 18(3): 304. doi: 10.1051/meca/2016062
31. Yuan Y, Liu B, Jia H, et al. Observation of uncommon elastic wave group velocity in common honeycomb structure and its potential for debonding detection. Applied Physics Letters. 2025; 126(2): 022202. doi: 10.1063/5.0237493

Appendix A. The influence of acoustic wave propagation in different number of honeycomb units on the detection results

To further verify the relationship between exciting-receiving distance and the honeycomb unit's width, honeycomb plates with different honeycomb core sizes were fabricated. The specimen (500 mm × 250 mm) was shown in **Figure A1a**. Both the honeycomb core and the skin are made of aluminum (Young's modulus E = 70 GPa, Poisson's ratio μ = 0.33, and density ρ = 2,700 kg/m^3) and bonded by epoxy resin. The honeycomb unit was shown in **Figure A1b;** the thickness of the skin and the height of the core are 0.5 mm and 20 mm, respectively. The wall of the core is 0.05 mm in thickness and 6 mm in side length. Meanwhile, the artificial debonding defects were introduced by removing the adhesive film between the skin and core at the corresponding debonding location. The diameter of the debonding defect is 35 mm, 25 mm, 20 mm, 10 mm, 8 mm, and 5 mm in order from the largest to the smallest.

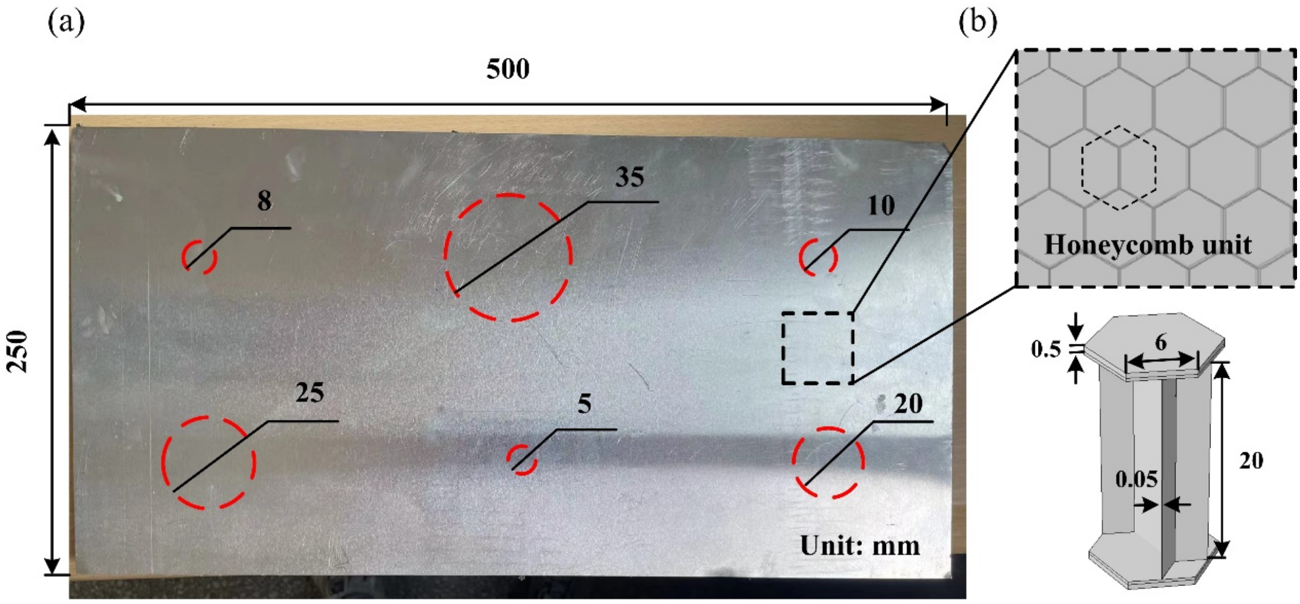

Figure A1. (a) The specimen; **(b)** Honeycomb unit.

According to the calculation method of the dispersion relation in Subsection 2.2, the dispersion relation of the honeycomb structure can be obtained in **Figure A2a**. Here, the dispersion curve was only calculated in the ΓK direction, and only the three band branches where modes A_0, R_{PS}, and R_{PA} are located that have a direct effect on band gap formation were presented in **Figure A2a**. It can be observed that a band gap appears from 30 kHz to 40 kHz between the band branches where modes R_{PS} and R_{PA} are located.

To demonstrate the existence of the band gap feature in the honeycomb structure, the TFR curves of intact and debonding areas were measured using the experimental platform described in Subsection 2.2. The measured TFR curves are shown in **Figure A2b**, where the red dash-dot line and black solid line denoted the TFR curves of intact and debonding areas, respectively. It can be observed that there is a steep fall in the range from 29 kHz to 37 kHz, and the minimum value of TFR reaches about −16 dB. The result demonstrated that there is a band gap at this frequency range. Compared to the TFR curve of the intact area, the TFR curve of the debonding area is nearly stable in the measured frequency band. It means that the band gap feature disappeared in the debonding area. Thus, it is further verified that the band gap feature can be applied to detect debonding in honeycomb structures.

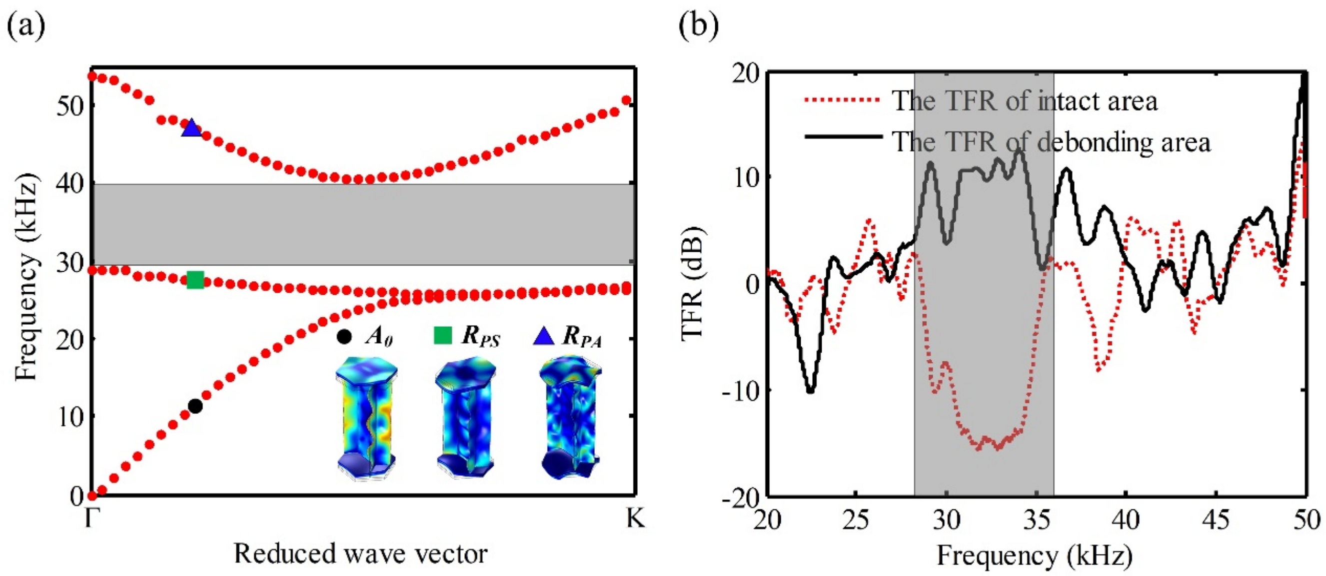

Figure A2. The dispersion curves and transmission frequency response (TFR) of the honeycomb structure: **(a)** Three types of the honeycomb structure below 55 kHz, which are modes R_{PS}, R_{PA} and A_0, respectively. There is a band gap between these branches in the frequency range from about 30 kHz to 40 kHz; **(b)** Measured TFR of intact and debonding areas of honeycomb structure (a steep fall in the range from 29 kHz to 37 kHz).

To further verify the relationship between the band gap feature and the number of acoustic waves propagating through the honeycomb units, we performed the same experiment as in the main text, as shown in **Figure A3a**. The exciting-receiving distance D was fixed at 40 mm on a 35-mm-diameter defect. The detection positions are divided into the following two types: Type 1: exciting point in the debonding area; receiving point is in the intact area, and d = 10 mm, 20 mm, and 30 mm from the edge of the debonding defect, which is about 1, 2, and 3 widths of the honeycomb unit (The honeycomb unit's width is about 10 mm when the side length of the honeycomb core is 6 mm). Type 2: Both exciting and receiving points are in the intact area; at this time, d = 40 mm. To improve the reliability of the test results, three measurements were carried out at each position, and the results were averaged to form a curve. The red, black, blue, and brown curves in **Figure A3b** represented the results at the distances of 10 mm, 20 mm, 30 mm, and 40 mm, respectively.

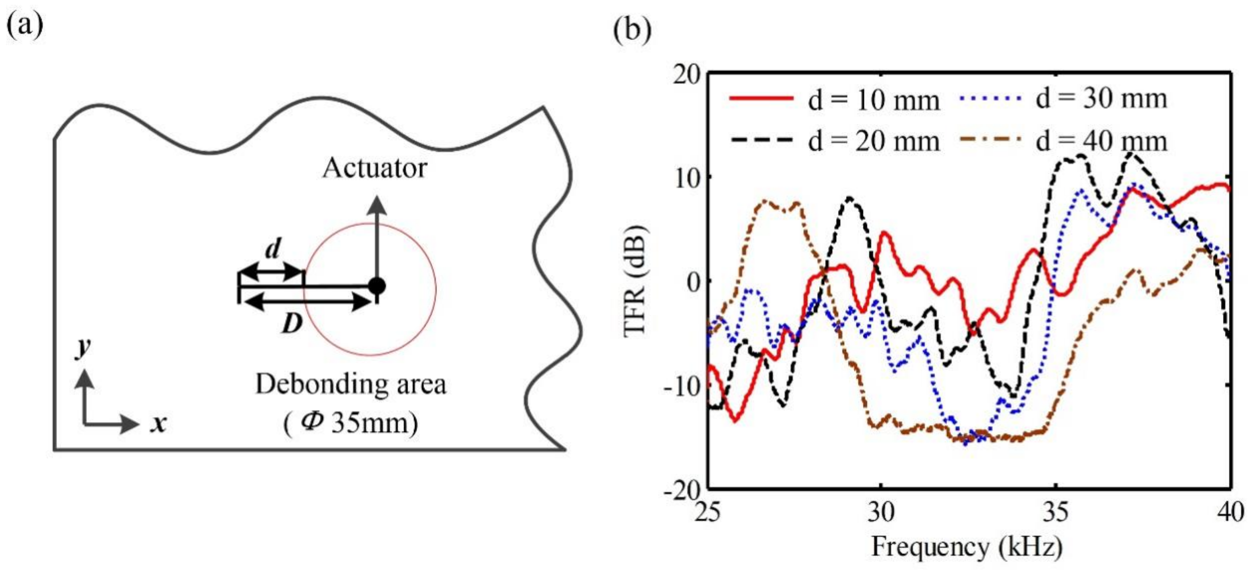

Figure A3. The influence of acoustic wave propagation in different numbers of honeycomb units on the detection results: **(a)** Experimental schematic of acoustic wave propagation in different numbers of honeycomb units; **(b)** Measured TFR curves with different numbers of honeycomb units (d = 10, 20, 30, 40 mm).

It can be observed that as the number of acoustic waves propagating through the honeycomb units increases, the attenuation of TFR in the bandgap range changes from 3 dB to 16 dB compared to the other frequency bands. This suggests that the formation of band gap features is related to the number of acoustic waves propagating through the honeycomb units, that is, the band gap feature can be faintly observed when the acoustic wave propagates through one or two honeycomb units. The band gap range and attenuation reach stability when the acoustic wave propagates through three or more honeycomb units.

Similar to the detection results in the main text for the honeycomb structure (side length of honeycomb core is 4 mm), the honeycomb structure, whose side length of honeycomb core is 6 mm, also requires the acoustic wave to propagate through a minimum distance of three honeycomb units to detect a stable band gap feature. Therefore, it is proved that the exciting-receiving distance D should be selected as $D \geq 3d_h$, where d_h is the width of the honeycomb unit.